Theoretical Analysis on Nonlinear Buckling, Post-Buckling of Slender Beams and Bi-Stable Mechanisms

Ke Wu, Gang Zheng

Theoretical Analysis on Nonlinear Buckling, Post-buckling of Slender Beams and Bi-stable Mechanisms

Ke Wu
Univ. Lille, Inria, CNRS
Centrale Lille, UMR 9189 CRIStAL
F-59000 Lille, France
Email: ke.wu@inria.fr

Gang Zheng *
Univ. Lille, Inria, CNRS
Centrale Lille, UMR 9189 CRIStAL
F-59000 Lille, France
Email: gang.zheng@inria.fr

Compliant Mechanisms (CMs) are used to transfer motion, force and energy, taking advantages of the elastic deformation of the involved compliant members. A branch of special type of elastic phenomenon called (post) buckling has been widely considered in CMs: avoiding buckling for better payload-bearing capacity and utilizing post-buckling to produce multi-stable states. This paper digs into the essence of beam's buckling and post-buckling behaviors where we start from the famous Euler–Bernoulli beam theory and then extend the mentioned linear theory into geometrically nonlinear one to handle multi-mode buckling problems via introducing the concept of bifurcation theory. Five representative beam buckling cases are studied in this paper, followed by detailed theoretical investigations of their post-buckling behaviors where the multi-state property has been proved. We finally propose a novel type of bi-stable mechanisms termed as Pre-buckled Bi-stable Mechanisms (PBMs) that integrate the features of both rigid and compliant mechanisms. The theoretical insights of PBMs are presented in detail. To the best of our knowledge, this paper is the first study on the theoretical derivation of the kinematic models of PBMs, which could be an important contribution to this field.

1 Introduction

1.1 Compliant mechanisms

Compliant Mechanisms (CMs) have gradually turned into a hot research spot over the last few years [1]. Conventional rigid mechanisms are designed to transfer motion, force and energy through the cooperative state of all the involved rigid links and kinematic pairs. Likewise, CMs are capable of realizing the same functions only through the elastic deformation of the built-in elementary flexible members. This unique concept offers several desired characteristics in terms of low cost and high performance [1] [2]: energy-saving operation [1]; more simplified manufacturing process [3]; less mechanical maintenance needed [2] and better motion precision achieved [4]. Due to these mentioned merits, CMs have been utilized in many mechanical applications, such as multi-stable mechanisms [5], constant-force-control mechanisms [6], compliant robotic actuation [8], energy-harvesting applications [9] and force sensors [10] serving as a promising type of alternative to conventional rigid mechanisms [1] [3].

1.2 Buckling and post-buckling of slender beams

1.2.1 From an engineering perspective

Flexible slender beams will present more diverse mechanical responses if buckling or post-buckling behavior occurs. Essentially, a slender beam tends to buckle into an unstable state if the axial loading reaches its critical value or equivalently its buckling limit, which is mainly due to imperfect geometry and off-axial loading or some external factors [11]. In all the mentioned scenarios, the lateral deformation will immediately occur and then sharply increase if the axial force is beyond the buckling limit. From an engineering point of view, the 'instability' nature of buckling would lie in the following three aspects: the sharply decreasing axial stiffness, the rapidly increasing lateral displacement and the unpredictable situations after the axial load reaches the critical load as it normally has three potential choices: one bucked state, another buckled state with symmetric geometry and even the unbuckled equilibrium state. For more theoretical details about buckling and post-buckling, the mentioned

*Corresponding author: Gang Zheng University of Lille, Inria, CNRS, Centrale Lille, UMR 9189 CRIStAL, F-59000 Lille, France, Tel: +33 3 59 57 79 53, Fax: +33 3 59 57 78 50.

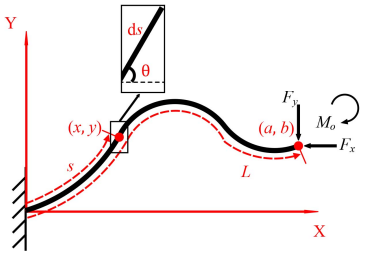

Fig. 1: General (post)-buckling of a slender straight beam

references here [12] are recommended.

However, this 'instability' nature would also present benefits if dialectically treating and making most of it. For example, slender structures used in civil engineering, marine engineering and aircraft engineering have therefore drawn a huge concern regarding elastic instability that may cause structural failure [13], which has to be avoided. On the other hand, the unique characteristics of buckling and post-buckling can also be utilized in some mechanical applications, such as bi-stable or multi-stable compliant mechanisms [14]. In the scope of this paper, we would like to characterize and **take advantages of these phenomena rather than simply avoid them** as the diverse mechanical response of buckling and post-buckling states would surely enrich some unexpectedly positive possibilities of current CMs.

1.2.2 The essence

The buckling theory has been intensively investigated since linear buckling theory (Euler buckling) was derived by Euler in 1744 [15] and further refined for higher modes by Lagrange in 1770 [16]. It's **worth noting** that the mentioned two authors both concluded their findings based on the famous beam equation by Bernoulli [17]:

$$EI\frac{\mathrm{d}\theta}{\mathrm{d}s} = M(s), \quad s \in [0,L] \tag{1}$$

which assumes the linear relationship between the beam curvature $\frac{\mathrm{d}\theta}{\mathrm{d}s}$ and the exerted moment M at (x, y) or equivalently s along the beam axis (see Fig. 1). $\theta(s)$ represents the orientation of the beam at s. E is the Young's modulus and I denotes the second moment of inertia of the cross section area; L denotes the beam length; $F_x(L)$, $F_y(L)$ and $M_o(L)$ are the *constant* forces and moment exerted at the beam end L (for simplicity we drop the dependency of L in the sequel). Therefore, the model regarding nonlinear buckling and post-buckling behavior (see Fig. 1) can be characterized by the following form: $EI\frac{\mathrm{d}\theta}{\mathrm{d}s} = F_x(b-y(s)) - F_y(a-x(s)) - M_o$ for $s \in [0,L]$ where F_y and M_o are involved only when analyzing post-buckling. Then, conducting differentiation of the above equation with respect to s results in the following equation:

$$EI\frac{\mathrm{d}^2\theta}{\mathrm{d}s^2} = -F_x\sin\theta + F_y\cos\theta, \quad s \in [0,L] \tag{2}$$

where $\frac{\mathrm{d}x}{\mathrm{d}s} = \cos\theta$ and $\frac{\mathrm{d}y}{\mathrm{d}s} = \sin\theta$ are utilized. Eq. (2) is in fact an ordinary differential equation (ODE) with respect to s to describe the orientation evolution of θ along s for $s \in [0,L]$. With different conditions defined at the point $s = 0$ and $s = L$, Eq. (2) becomes as a typical two-point boundary value problem (BVP). Mathematically, the existence of solution for a general BVP is a difficult problem. However, due to the fact that (2) is arisen from engineering applications, therefore it is well-posed with different but coherent boundary conditions (B.C.), which are determined by variant end-support cases of beam, as shown in Fig. 2: free end, pinned end, roller, fixed end, sliding end, etc. Summarizing what we have stated

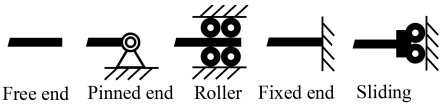

Fig. 2: Different types of beam ends

above, buckling problem is essentially to analyze a two-point BVP (2) without involving F_y under different B.C., which yields the similar form of the following type:

$$\begin{aligned} &\text{D.E. } EI\frac{\mathrm{d}^2\theta}{\mathrm{d}s^2} = -F_x\sin\theta, \quad s \in [0,L] \\ &\text{B.C. } g\big(\theta(0),\theta'(0),\theta(L),\theta'(L)\big) = 0 \end{aligned} \tag{3}$$

where $g \in \mathbb{R}^2$ represents different independent boundary conditions defined at $s = 0$ and $s = L$.

Unlike buckling problem where only the X-axis force F_x exists, post-buckling problems might contain external F_y and M_o, and this can be formulated as follows:

$$\begin{aligned} &\text{D.E. } EI\frac{\mathrm{d}^2\theta}{\mathrm{d}s^2} = -F_x\sin\theta + F_y\cos\theta \\ &\text{B.C. } g\big(\theta(0),\theta'(0),\theta(L),\theta'(L)\big) = 0 \end{aligned} \tag{4}$$

We would like to emphasize that BVPs (3) and (4) may have different solutions under the same boundary conditions although it looks so much like the simple single-solution beam-deflection problem, which in this case corresponds to the different geometries of the slender beam subjected to an axial load F_x above some buckling limit (see Fig. 3). Essentially speaking, this is because BVP (3) has gone through a *bifurcation phenomenon*, and we would like to briefly recall the definition of *bifurcation* [18] here:

Definition 1. *In dynamical system described by an ODE as* $\frac{dx}{dt} = f(x,p)$ *with* $x \in \mathbb{R}^{n_x}$ *and* $p \in \mathbb{R}^{n_p}$*, a bifurcation solution of* x *occurs when a small smooth change of* p *causes a sudden "qualitative" or topological change of* x *in its behavior.*

In our case, BVP (3) can be regarded as the *dynamical system* as we can always consider BVP (3) as a dynamical system with respect to s. In such an ODE, *bifurcation parameter* refer to the axial loading F_x which may trigger the *sudden "qualitative" or topological change of* θ. This definition theoretically explains the possible sudden and rapid geometry change of slender structures when the axial load reaches the critical limit, which in the scope of this paper is *buckling*.

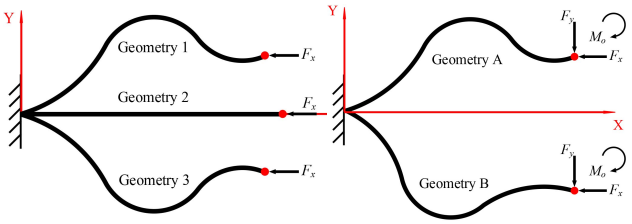

(a) Buckling geometry (b) Post-buckling geometry

Fig. 3: Schematic geometries of (post)-buckling of beams

Therefore, BVP (3) can describe the buckling phenomenon as shown in Fig. 3a: the buckled beam will always have two potential geometries (see Geometry 1 and Geometry 3) and more importantly it is also possible for the beam to stay axially equilibrium (Geometry 2). Note we don't consider any imperfections of the studied beam in this paper, but if we do (for instance, a small initial curvature of the beam) logically the beam will result in one buckled state (where Fig. 3a does not apply) [19].

Supposing the beam has buckled and presented the potential Geometry 1 or Geometry 3 as displayed in Fig. 3a, the beam will go through post-buckling phenomenon under some extra beam-end loading (F_y and M_o) and eventually reached Geometry A or Geometry B respectively as shown in Fig. 3b. Obviously, BVP (4) can be utilized to describe this post-buckling behavior. A bifurcation diagram (Fig. 4) is used to explain the process of buckling and post-buckling where in particular Path 1 is due to the continuous increase of F_x whereas Path 2 and Path 3 are possibly the combined results of F_x, F_y and M_o. Note that there always exists a point $s^* \in [0, L]$ such that the lateral displacement of this point $y(s^*)$ will go through a bifurcation phenomenon as shown in Fig. 4 and Fig. 6.

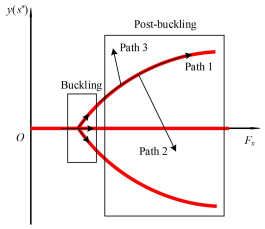

Fig. 4: Schematic bifurcation diagram of (post)-buckling

1.2.3 State of the art

As we have explained in the above that buckling and post-buckling problems can be modeled as BVPs under different B.C. Therefore, two main methodologies have been reported in the literature. The first method is to solve BVPs analytically, relying on Euler buckling theory to find the critical loads [20]. Due to the fact that those BVPs are normally nonlinear when large deformation occurs, therefore elliptic integral approach has been applied in the above mentioned references to handle non-linearity, which make those methods not really analytic. Besides, another methodology is to solve BVPs purely via an approximate manner. In such a branch, one brilliant work [21] completed in 1997 has turned out to be the first comprehensive contribution of solving buckling and post-buckling problems under different beam-end conditions (which are essentially different BVPs) via a numerical scheme: shooting method. [22] utilized 3-order Taylor series to simplify the original 'buckling' ODE to a linear one (see Eq. (35) and Eq. (40) in [22]) and then derived a closed-form solution to the nonlinear post-buckling problem which is accurate enough up to a rise-to-span ratio of about 0.3 compared to elliptic-integral solutions. Logically, the higher the order of the polynomials is, the closer the results are to analytical results (see Fig. 9 in [22]). The contributors of [23] proposed a differential quadrature based iterative numerical integration method to solve post-buckling nonlinear ODE where six representative cases have been studied. In this paper, we aim to offer a **more straightforward, easy-to-follow and efficient** method to characterize the **exact** buckling and post-buckling behavior of slender beams **without adopting elliptic-integral-based solutions** to BVPs (3) and (4).

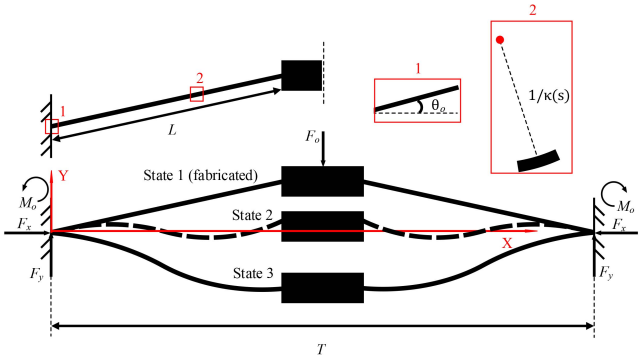

Fig. 5: Schematic operation of a bi-stable mechanism

1.3 Compliant bi-stable mechanisms

Compliant bi-stable mechanisms are a special branch of CMs which has two stable equilibrium states [14] (see State 1 and State 3 in Fig. 5). This special type of mechanisms is potential alternative for a wide variety of mechanical applications: sensors [24]; state switches [25], relays [26], reconfigurable robotic system [27], landing gear mechanisms [28], and devices for vibration energy harvesting [29].

The transition between these two stable equilibrium states is essentially the operational process of these mechanisms, and they can stay stable without any power input in these states. Note that during the transition, the mechanisms often need to go through an unstable equilibrium state which is State 2 in Fig. 5. At this unstable position, the system would jump into either of the mentioned stable equilibrium states if any disturbance occurs, which again triggers the concept of *bifurcation phenomenon* presented in Section 1.2.2.

Similar to BVPs (3) and (4), a typical bi-stable mechanism as shown in Fig. 5 can be theoretically described as the following two BVPs (5) and (6). The equilibrium states of

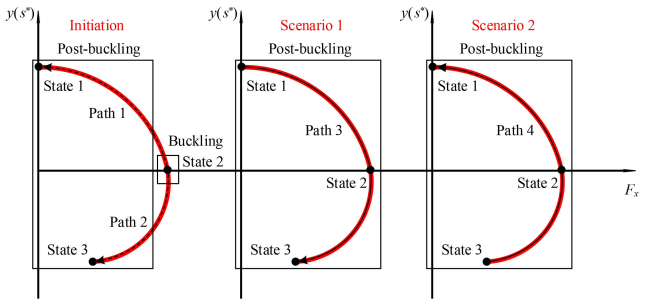

Fig. 6: Schematic bifurcation of bi-stable mechanisms

the bi-stable system can be formulated below:

$$\begin{aligned} &\text{D.E.} \quad \frac{\mathrm{d}^2\theta}{\mathrm{d}s^2} = f(\frac{\mathrm{d}\theta}{\mathrm{d}s}(s),\theta(s),F_x,M_o,E,I(s),L,T) \\ &\text{B.C.} \quad g\left(\theta(0),\theta'(0),\theta(L),\theta'(L)\right)=0 \end{aligned} \tag{5}$$

and the entire in-equilibrium transition process between State 1 and State 3 are described below:

$$\begin{aligned} &\text{D.E.} \quad \frac{\mathrm{d}^2\theta}{\mathrm{d}s^2} = f(\frac{\mathrm{d}\theta}{\mathrm{d}s}(s),\theta(s),F_o,F_x,F_y,M_o,E,I(s),L,T) \\ &\text{B.C.} \quad g\left(\theta(0),\theta'(0),\theta(L),\theta'(L)\right)=0 \end{aligned} \tag{6}$$

where F_o denotes the actuation force which drives the system from one equilibrium state to another; $I(s)$ implies that BVPs (5) and (6) can define bi-stable systems with beams of uniformly varying cross section (in other words, $I(s)$ needs to be continuous and derivable); T stands for the horizontal distance between the two fixed bases.

Now we are ready to start our analysis on the basis of BVP (5): at State 1, F_x and M_o both equal 0 as they are in the undeformed shape; State 2 is the unstable one and may jump to State 1 or State 3 if any random disturbance occurs, which means the whole system is at the buckling initiation, and more importantly, F_x would possibly reach its maximum. Fig. 6 explains the essence of how bi-stable mechanisms work by introducing the *bifurcation diagram*. As shown in Fig. 6, State 2 actually refers to buckling initiation state, and it can switch to State 1 or State 3 through Path 1 or Path 2 under a corresponding disturbance, which is termed as **Initiation**. In practice, bi-stable mechanisms would normally start to operate from State 1 (Scenario 1) or State 3 (Scenario 2) rather than Initiation stage (State 2) where it can be clearly noticed that the starting points of Scenario 1 and Scenario 2 are actually the buckling consequences of Initiation stage. Logically, Scenario 1 is a post-buckling process from State 1 to State 3 through Path 3. Similarly, Scenario 2 is also a post-buckling process from State 3 to State 1 through Path 4. To sum up, we can conclude that the operational processes of bi-stable mechanisms are essentially **post-buckling behaviors** of the bi-stable systems.

With the conclusion reached from the above analysis, we have already found out that bi-stable mechanisms are heavily concerned with buckling and post-buckling phenomena. Therefore, this paper essentially investigates the buckling and post-buckling problems of via digging into BVPs (3) and (4). Mathematically, to solve this problem, we can normally have two types of strategies: analytical solutions and numerical solutions. However for general nonlinear BVPs, it is difficult to find analytical solutions. Therefore, this paper adopts collocation technique as a numerical method to solve this nonlinear BVP.

1.4 Collocation method

In this paper, we employ collocation method to solve the mentioned problems in previous paragraphs. As reported in the literature of applied mathematics, collocation method has already been a widely accepted option of solving two-point BVPs, and it essentially conducts collocation with several continuous polynomial functions to approximate the target unknown function under given boundary conditions [30] [31]. To recall it, we would like to briefly explain how BVPs (3) and (4) are handled using collocation method.

Firstly, we rearrange BVPs (3) and (4) into the following general form for simplicity:

$$\begin{aligned} &\text{D.E.} \quad \frac{\mathrm{d}^2\theta}{\mathrm{d}s^2} = f(s,\frac{\mathrm{d}\theta}{\mathrm{d}s},\theta...) \\ &\text{B.C.} \quad g\left(\theta(0),\theta'(0),\theta(L),\theta'(L)\right)=0 \end{aligned} \tag{7}$$

Then we can solve the above BVPs via collocation method through a local manner.

1.4.1 Basic idea of approximation

Generally speaking, by dividing the interval $[0,L]$ into $i+1$ points $0=s_0<s_1<\cdots<s_i=L$ (named as collocation points), collocation method approximates the solution of the BVP via linear combination of well-chosen basis functions by satisfying D.E. and B.C. at all collocation points.

Precisely, denote by $\Theta(s)$ the approximate solution of (7), and suppose that a cubic polynomial $p_k(s)$ is chosen to approximate the solution θ of (7) on each sub-interval $[s_{k-1}, s_k]$, i.e., $\Theta(s)=\sum_{k=1}^{i} p_k(s)$ where

$$p_k(s)=\begin{cases} b_{k0}+b_{k1}s+b_{k2}s^2+b_{k3}s^3, \ \forall s\in[s_{k-1},s_k] \\ 0, \qquad\qquad\qquad\qquad \text{otherwise} \end{cases} \tag{8}$$

with b_{kj} for $0\le j\le 3$ being the 4 unknown polynomial coefficients on the kth interval. In total, we have $4i$ unknown parameters to be identified. Clearly, $\Theta(s)$ should satisfy the D.E. in (7) for all collocations points, and this yields the following $3i$ algebraic equations to be fulfilled:

$$\begin{aligned} &\frac{\mathrm{d}^2\Theta}{\mathrm{d}s^2}(s_{k-1}) = f(s_{k-1},\frac{\mathrm{d}\Theta}{\mathrm{d}s}(s_{k-1}),\Theta(s_{k-1})) \\ &\frac{\mathrm{d}^2\Theta}{\mathrm{d}s^2}(\bar{s}^k_{k-1}) = f(\bar{s}^k_{k-1},\frac{\mathrm{d}\Theta}{\mathrm{d}s}(\bar{s}^k_{k-1}),\Theta(\bar{s}^k_{k-1})) \\ &\frac{\mathrm{d}^2\Theta}{\mathrm{d}s^2}(s_k) = f(s_k,\frac{\mathrm{d}\Theta}{\mathrm{d}s}(s_k),\Theta(s_k)) \end{aligned} \tag{9}$$

where $\bar{s}_{k-1}^{k} = \frac{s_{k-1}+s_k}{2}$.

Note that the approximated solution $\Theta(s)$ is a combination of a series of local polynomials, therefore additional equation should be imposed to guarantee the continuity at all collocation points, i.e., $p_{k-1}(s_{k-1}) = p_k(s_{k-1}), \forall k \in [2,i]$. Hence we have the above $i-1$ algebraic equations due to the continuity conditions. Together with the 2-dimensional B.C. in (7), we finally obtain a set of algebraic equations with dimension $3i+i-1+2 = 4i+1$, which will be used to compute those $4i$ unknowns parameter b_{kj} defined in (8).

Furthermore, we can take one step further to ensure the differentiability, i.e. $\Theta(s) \in C^1$, by imposing the following derivative continuity conditions at all collocation points: $\frac{\mathrm{d}p_{k-1}}{\mathrm{d}s}(s_{k-1}) = \frac{\mathrm{d}p_k}{\mathrm{d}s}(s_{k-1}), \forall k \in [2,i]$. which gives another $i-1$ equations, yielding altogether $4i+1+i-1 = 5i$ algebraic equations available.

In summary, collocation method enables us to solve the $4i$ unknowns b_{kj} based on the $4i+1$ or $5i$ equations which can be numerically solved via Newton-Raphson method.

It is worth noting that numerical tools would always need an initial guess to start its iterative computation which might play an important role in the convergence and local minima. In our context, we can have two different ways to set the initial values of b_{kj}:

1. **Direct way:** We randomly initialize the values of b_{kj}, which yields a random shape of $\Theta(s)$.
2. **Indirect way:** We choose a globally initial guess for $\Theta(s)$, which yields the corresponding b_{kj} for every cubic polynomial $p_k(s)$.

The direct way is suitable for the scenario where the problem tends to have only one single solution, i.e., global minima. The indirect way goes for the scenario where we reasonably initialize the initial guess (possibly near the final solution) for the final solution via using the existing information, and it is suitable to treat local minima case which is exactly the buckling topic discussed in this paper. We would like to remark that the discretization idea of this proposed collocation method looks similar to that of classic FEA, but they are essentially two different strategies to solve beam-deflection problems. In fact, FEA does not have a global governing equation to describe the deformation, therefore it has to use quite a lot finer mesh elements to handle large deformation. Conversely, this paper proposes a global governing equation to describe the large beam-deflection problems for which collocation method is used to approximate its solution. Consequently, it is possible to have a precise approximation of the solution by even using a low-order polynomial.

1.4.2 Final geometry

Finally, as long as $\theta(s)$ is obtained, the deformed beam shape $x(s)$ and $y(s)$ can be obtained using: $x(s) = \int_0^s \cos(\theta(\xi))\mathrm{d}\xi$ and $y(s) = \int_0^s \sin(\theta(\xi))\mathrm{d}\xi$.

1.5 Newton-Raphson method

As reported in the literature of applied mathematics, there are several methods to handle nonlinear equations or system of equations. In this paper, we would like to proceed with a commonly used method called Newton-Raphson method for these problems. Here, a brief recap is presented to solve a general nonlinear equation or a system of nonlinear equations $f(x) = 0$: $x_i = x_{i-1} - \frac{f(x_{i-1})}{f'(x_{i-1})}$, where x_i in the ith can be calculated from the $i-1$th trial x_{i-1} and $f'(x_{i-1})$ can be numerically solved using Newton's divided difference formula. After the convergence (in practice the convergence criteria is set as $||x_{i+1} - x_i|| \leq \varepsilon$ where ε is a predefined threshold), we can finally obtain the solution x to $f(x) = 0$. Note that x can be a vector in this method.

1.6 Structure of the paper

We first present a straightforward numerical strategy to solve buckling and post-buckling problems of slender beams where several basic Euler-buckling and its extended cases are studied and reliable FEA results are shown to compare and verify our method. Then, based on the theoretical analysis, we therefore systematically propose a new type of bi-stable mechanisms, **Pre-buckled Bi-stable Mechanisms (PBMs)** with the theoretical insights provided regarding PBM design and optimization.

2 Characterization of nonlinear buckling phenomenon

In this section, we are going to study five cases (Case 1 to Case 5) of non-linear buckling phenomena. They are actually five different cases of Eq. 3 under different boundary conditions. In these five cases, the initial axis of the beam is required to coincide with x-axis for buckling study, which means the beam does not have initial curvature. Note that the nonlinear buckling behavior studied in the following paper refers to the **first-order** nonlinear buckling if without being specified. Briefly speaking, the buckling behavior of slender structures contains many (theoretically infinite if not considering the maximum stress limit of these structures) modes of shapes and buckling loads. The first-order buckling refers to the buckling phenomenon with simplest shape which is most likely to occur and triggered by the least buckling load [15].

2.1 Case 1: classic buckling problem

This case aims to study a slender beam with one end fixed to the base and the other end only subjected to an axial force F_x without any other constraints, which is graphically displayed in Fig. 7. Starting from Eq. (1), we can obtain

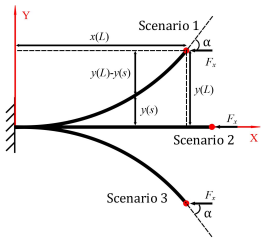

Fig. 7: The schematic beam deformation of Cases 1 and 3

$EI\frac{\mathrm{d}\theta}{\mathrm{d}s} = M(s) = F_x(y(L) - y(s))$ whose differentiation gives:

$$EI\frac{\mathrm{d}^2\theta}{\mathrm{d}s^2} = -F_x \sin\theta(s) \tag{10}$$

Rearranging (10), we will have $\frac{1}{2}EI(\frac{\mathrm{d}\theta}{\mathrm{d}s})^2 - F_x\cos\theta(s) = C$, where C is an unknown constant which can be determined by the boundary conditions. Precisely,

$$C = \frac{1}{2}EI(\frac{\mathrm{d}\theta}{\mathrm{d}s}(L))^2 - F_x\cos\theta(L) = -F_x\cos\alpha \tag{11}$$

where $EI\frac{\mathrm{d}\theta}{\mathrm{d}s}(L) = 0$ and $\theta(L) = \alpha$, and α is an unknown parameter to be determined. Similarly,

$$C = \frac{1}{2}EI(\frac{\mathrm{d}\theta}{\mathrm{d}s}(0))^2 - F_x\cos\theta(0) = \frac{F_x^2}{2EI}y(L)^2 - F_x \tag{12}$$

where $EI\frac{\mathrm{d}\theta}{\mathrm{d}s}(0) = F_x y(L)$ and $\theta(0) = 0$. Rearranging the above equations drives us to have $\frac{\mathrm{d}\theta}{\mathrm{d}s} = \pm\sqrt{\frac{2F_x}{EI}(\cos\theta(s) - \cos\alpha)}$, which actually results in three possibilities. If $\theta(s) = 0$, then we can easily obtain $\alpha = \theta(s) = 0$ and $\frac{\mathrm{d}\theta}{\mathrm{d}s}(s) = 0$, which leads to Scenario 2 as shown in Fig. 7. Otherwise, we will have $\frac{\mathrm{d}\theta}{\mathrm{d}s} = +\sqrt{\frac{2F_x}{EI}(\cos\theta(s) - \cos\alpha)}$ if $\alpha > 0$ and $\frac{\mathrm{d}\theta}{\mathrm{d}s} = -\sqrt{\frac{2F_x}{EI}(\cos\theta(s) - \cos\alpha)}$ if $\alpha < 0$, which clearly corresponds to Scenarios 1 and 3 as shown in Fig. 7. Here, we only take the case $\alpha > 0$ as an example to finish the rest deduction and logically solving the case $\alpha < 0$ follows the same procedure. Assume $f(\alpha)$ as:

$$f(\alpha) = \int_0^{\alpha^-} \frac{1}{\sqrt{\frac{2F_x}{EI}(\cos\theta(s) - \cos\alpha)}}\mathrm{d}\theta - \int_{0^+}^{L^-}\mathrm{d}s \tag{13}$$

then we can obtain the value of α by solving $f(\alpha) = 0$ under Newton-Raphson method. If we consider (11) and (12) together, we can easily derive the expression for $y(L)$: $y(L) = \sqrt{(1-\cos\alpha)\frac{2EI}{F_x}}$.

So far, we have got all the information needed of the boundary conditions: $\theta(0) = 0$, $\frac{\mathrm{d}\theta}{\mathrm{d}s}(0) = \frac{F_x y(L)}{EI}$, $\theta(L) = \alpha$ and $\frac{\mathrm{d}\theta}{\mathrm{d}s}(L) = 0$. Differentiating (10) twice ends up with a fourth-order ODE: $EI\frac{\mathrm{d}^4\theta}{\mathrm{d}s^4} + F_x(-\sin\theta(s)(\frac{\mathrm{d}\theta}{\mathrm{d}s})^2 + \cos\theta(s)\frac{\mathrm{d}^2\theta}{\mathrm{d}s^2}) = 0$. Logically, we can have the final solution of $\theta(s)$ via solving the obtained ODE using collocation method.

2.2 Case 2: classic buckling problem considering gravity

In this case, we take gravity into account when dealing with the classic buckling problem. Based on the loading condition as shown in Fig. 8, we can have the fundamental first-order ODE that comes from Eq. (1): $EI\frac{\mathrm{d}\theta}{\mathrm{d}s} = F_x(y(L) - y(s)) + \int_s^L q_x(s)(y(r) - y(s))\mathrm{d}r$.

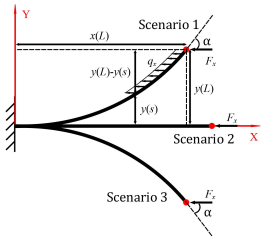

Fig. 8: The schematic beam deformation of Case 2

Differentiating this equation, we then reach:

$$EI\frac{\mathrm{d}^2\theta}{\mathrm{d}s^2} = -F_x\sin\theta(s) + q_x\sin\theta(s)(s-L) \tag{14}$$

with the boundary conditions: $\theta(0) = 0$ and $\frac{\mathrm{d}\theta}{\mathrm{d}s}(L) = 0$. Obviously, we are not able to manipulate (14) like what we do for Case 1, which means α and $y(L)$ are unknown and therefore can not be used for setting up the above boundary conditions.

When applying numerical method, the numerical trial always starts from an initial guess and then reaches the final numerical solution by satisfying some given boundary conditions [32] [33]. Therefore, we need to choose a good initial guess to guide the numerical process especially when solving multi-solution problems.

As for Case 2, $\theta(s) = 0$ can be easily found as one of the solutions that corresponds to Scenario 2 as displayed in Fig. 8. Similar to Case 1, Scenarios 1 and 3 here are symmetric to each other so we just go through the deduction of the former as an example. If we take a closer look at the above deduced fundamental first-order ODE, we may have an intuition of the form of $\theta(s)$ which therefore can be utilized as its initial guess $\theta(s)_{ig} = a(s-L)^2 + \alpha_{ig}$, where a is an undetermined parameter and α_{ig} denotes the initial guess of α. They could be both set as a relatively small number for the first trial. Logically, $\frac{\mathrm{d}\theta}{\mathrm{d}s}(s)$ follows the form below: $\frac{\mathrm{d}\theta}{\mathrm{d}s}(s)_{ig} = -2a(s-L)$. By slightly tuning the values of a and α_{ig} for the initial guesses, we can easily find the solution of $\theta(s)$ via collocation method.

2.3 Case 3: classic buckling problem considering uniformly varying cross section

In this case, we aim to consider the buckling phenomenon of a slender beam with uniformly varying cross section as displayed in Fig. 7. Likewise, we are not able to find the values of α and $y(L)$ beforehand so we need to follow the procedure proposed in Case 2. First, we need to be ready with the definition of Case 3: $EI(s)\frac{\mathrm{d}\theta}{\mathrm{d}s} = M(s) = F_x(y(L) - y(s))$, where $I(s)$ is the function of s. This implies

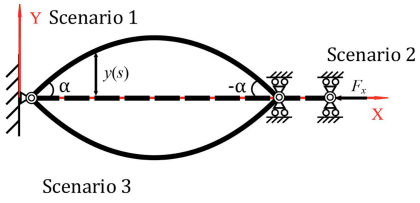

Fig. 9: The schematic beam deformation of Case 4

the cross section of the beam varies respect to s, and if $I(s)$ is continuous and deliverable (uniformly varying cross section), we can arrive at the differentiation result of the above equation: $EI'(s)\frac{d\theta}{ds} + EI(s)\frac{d^2\theta}{ds^2} = -F_x \sin\theta(s)$, with the following boundary conditions: $\theta(0) = 0, \frac{d\theta}{ds}(L) = 0$. Similarly, we set up the same initial guesses of the same formulation in Section 2.2 for the obtained BVP and we can then reach the final solution of $\theta(s)$ using collocation method.

2.4 Case 4: classic buckling problem about moving revolute joints at the both ends

In this case, we study the beam buckling phenomenon with revolute joints at the both ends. **Note** that this case can be considered as a simple combined one of rigid and flexible mechanisms. We first start with its fundamental equation: $EI\frac{d\theta}{ds} = M(s) = -F_x y(s)$. Then, differentiating it results in:

$$EI\frac{d^2\theta}{ds^2} = -F_x \sin\theta(s) \tag{15}$$

Rearranging (15), we will obtain: $\frac{1}{2}EI(\frac{d\theta}{ds})^2 - F_x\cos\theta(s) = C$, where C is an unknown parameter which can be determined by the boundary conditions. Precisely,

$$C = \frac{1}{2}EI(\frac{d\theta}{ds}(0))^2 - F_x\cos\theta(0) = -F_x\cos\alpha \tag{16}$$

where $EI\frac{d\theta}{ds}(0) = 0$ and $\theta(0) = \alpha$, and α is an unknown parameter to be determined. Similarly, $C = \frac{1}{2}EI(\frac{d\theta}{ds}(L))^2 - F_x\cos\theta(L) = -F_x\cos\alpha$, where $EI\frac{d\theta}{ds}(L) = 0$ and $\theta(L) = 0$. Rearranging this equation with (16) drives us to have: $\frac{d\theta}{ds} = \pm\sqrt{\frac{2F_x}{EI}(\cos\theta(s) - \cos\alpha)}$ It is obvious that the obtained differential system has three solutions: if $\theta(s) = 0$, then we can easily obtain $\alpha = \theta(s) = 0$ and $\frac{d\theta}{ds}(s) = 0$, which leads to Scenario 2 as shown in Fig. 9. Otherwise, we will have: $\frac{d\theta}{ds} = -\sqrt{\frac{2F_x}{EI}(\cos\theta(s) - \cos\alpha)}$ if $\alpha > 0$ and $\frac{d\theta}{ds} = +\sqrt{\frac{2F_x}{EI}(\cos\theta(s) - \cos\alpha)}$ if $\alpha < 0$, which clearly corresponds to Scenarios 1 and 3 as shown in Fig. 9. For idea demonstration, we just take the case of $\alpha > 0$ as an example, and solving the case of $\alpha < 0$ has the same procedure. Assuming $f(\alpha)$ as:

$$f(\alpha) = \int_{\alpha^-}^{-\alpha^+} -\frac{1}{\sqrt{\frac{2F_x}{EI}(\cos\theta(s) - \cos\alpha)}}d\theta - \int_{0^+}^{L^-} ds \tag{17}$$

Therefore, $f(\alpha) = 0$ can be logically solved via Newton-Raphson method to obtain the value of α. Then, we can start to handle the four-order system of (15):

$$EI\frac{d^4\theta}{ds^4} + F_x(-\sin\theta(s)(\frac{d\theta}{ds})^2 + \cos\theta(s)\frac{d^2\theta}{ds^2}) = 0 \tag{18}$$

as all the boundary conditions are known at this point: $\theta(0) = \alpha$, $\frac{d\theta}{ds}(0) = 0$, $\theta(L) = -\alpha$ and $\frac{d\theta}{ds}(L) = 0$. Using collocation method to reach the solution of (18) yields our final target $\theta(s)$.

For the Nth ($N = 1, 2, 3...$) mode of the buckling behaviors [15] that is displayed in Fig. 10, we just need to follow the strategy: $f(\alpha) = \int_{\alpha^-}^{-\alpha^+} -\frac{1}{\sqrt{\frac{2F_x}{EI}(\cos\theta(s) - \cos\alpha)}}d\theta - \int_{0^+}^{\frac{L}{N}^-} ds$. As long as α is obtained, revisiting (18) will provide the corresponding Nth-mode solution of $\theta(s)$.

2.5 Case 5: classic buckling problem about moving fixed constraints at the both ends

In this case, we aim to investigate the classic buckling problem about moving fixed constraints at the both ends. **Note** that similar to Case 4, this case can also be considered as a simple combined one of rigid and flexible mechanisms as well. We need to start with its fundamental equation for explaining the three scenarios shown in Fig. 11: $EI\frac{d\theta}{ds} = M(s) = -F_x y(s) + M_o$, where M_o logically equals 0 only if the slender beam is axially equilibrium under the condition of Scenario 2. Differentiating this equation, we have: $EI\frac{d^2\theta}{ds^2} = -F_x \sin\theta(s)$, with the boundary conditions: $\theta(0) = 0, \theta(L/2) = 0$. Likewise, $\theta(s) = 0$ can be easily found as one of the solutions that corresponds to Scenario 2 as displayed in Fig. 11. To handle Scenario 1, we set up appropriate initial guesses for the above deduced BVP: $\theta(s)_{ig} = -\frac{16a}{L^2}(s - \frac{L}{4})^2 + a$ and $\frac{d\theta}{ds}(s)_{ig} = -\frac{32a}{L^2}(s - \frac{L}{4})$, where a is an unknown parameter to be determined, we then can obtain the solution of $\theta(s)$ via tuning a from a small value. Scenario 3 can be explained in the same manner as well.

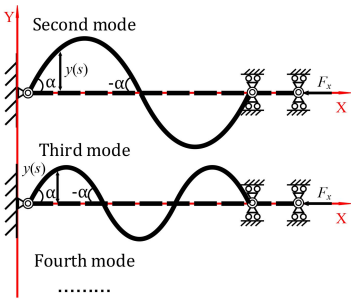

Fig. 10: The schematic beam deformation of Case 5

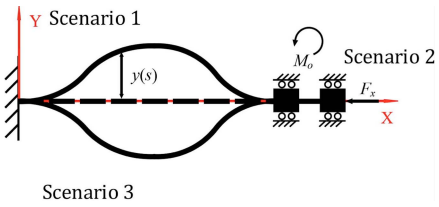

Fig. 11: The schematic beam deformation of Case 5

3 Characterization of non-linear post-buckling phenomenon

In the last section, we have covered five common cases of classic buckling problems so we will move forward to characterize their post-buckling behaviors where three representative cases (Case 6 to Case 8) are studied. Essentially, these three different cases are derived from Eq. 4 with different boundary conditions.

3.1 Case 6: post-buckling behavior of a fixed constraint at one end

This case actually is a further study of Case 1, which deals with its post-buckling behavior as shown in Fig. 12. Suppose the post-buckling behavior starts from point A through point B, and ends at point C. We first need to manipulate its governing equation (1) into a handy state: $EI\frac{\mathrm{d}\theta}{\mathrm{d}s} = M(s) = F_x(y(L)-y(s)) - F_y(x(L)-x(s))$. Differentiating this equation results in:

$$EI\frac{\mathrm{d}^2\theta}{\mathrm{d}s^2} = -F_x\sin\theta(s) + F_y\cos\theta(s) \tag{19}$$

Rearranging (19) leads to the following:

$$\frac{1}{2}EI(\frac{\mathrm{d}\theta}{\mathrm{d}s})^2 - F_x\cos\theta(s) - F_y\sin\theta(s) = C \tag{20}$$

where C is to be determined by the boundary conditions. Precisely, we have the following relation:

$$C=\frac{1}{2}EI(\frac{\mathrm{d}\theta}{\mathrm{d}s}(0))^2-F_x\cos\theta(0)-F_y\sin\theta(0)=\frac{1}{2}EI(\frac{\mathrm{d}\theta}{\mathrm{d}s}(0))^2-F_x \tag{21}$$

where $\theta(0)=0$, and $\frac{\mathrm{d}\theta}{\mathrm{d}s}(L)$ stays unknown for this moment. Similarly we get $C=\frac{1}{2}EI(\frac{\mathrm{d}\theta}{\mathrm{d}s}(L))^2-F_x\cos\theta(L)-F_y\sin\theta(L)=-F_x\cos\alpha-F_y\sin\alpha$ where $EI\frac{\mathrm{d}\theta}{\mathrm{d}s}(L)=0$ and $\theta(L)=\alpha$, and α stays unknown for this moment. Substituting this equation into (20) yields:

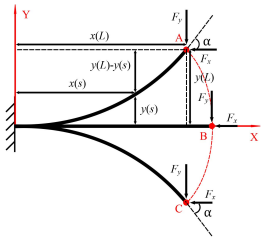

Fig. 12: Case 6: post-buckling behavior of Case 1

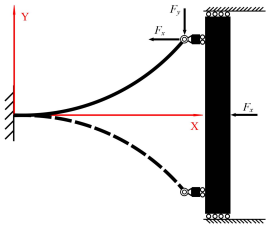

Fig. 13: Conceptual design of the mechanism of Case 6

$$\frac{\mathrm{d}\theta}{\mathrm{d}s} = \pm\sqrt{\frac{2F_x}{EI}(\cos\theta(s)-\cos\alpha)+\frac{2F_y}{EI}(\sin\theta(s)-\sin\alpha)} \tag{22}$$

Obviously, $\theta(s)=0$ and $F_y=0$ is one unique solution (that is point B in Fig. 12) of (22) as well as (19). If $\alpha>0$, we will have:

$$f(\alpha,F_y)=\int_0^{\alpha^-}\frac{1}{\sqrt{\frac{2F_x}{EI}(\cos\theta(s)-\cos\alpha)+\frac{2F_y}{EI}(\sin\theta(s)-\sin\alpha)}}\mathrm{d}\theta - \int_0^{L^-}\mathrm{d}s \tag{23}$$

Given α or F_y, it can be directly solved using Newton-Raphson method. Similarly, if $\alpha<0$, we will arrive at: $f(\alpha,F_y)=\int_0^{\alpha^+}\frac{-1}{\sqrt{\frac{2F_x}{EI}(\cos\theta(s)-\cos\alpha)+\frac{2F_y}{EI}(\sin\theta(s)-\sin\alpha)}}\mathrm{d}\theta - \int_0^{L^-}\mathrm{d}s$. Obviously, it can be solved in the same manner using Newton-Raphson method. As long as α and F_y are known, we can logically find out the expression and its value of $\frac{\mathrm{d}\theta}{\mathrm{d}s}(0)$ by rearranging (21): $\frac{\mathrm{d}\theta}{\mathrm{d}s}(0)=\pm\sqrt{\frac{2}{EI}(F_x-F_x\cos\alpha-F_y\sin\alpha)}$. So far, the essential information of the boundary conditions can be summarized as: $\theta(0)=0$, $\frac{\mathrm{d}\theta}{\mathrm{d}s}(0)=\pm\sqrt{\frac{2}{EI}(F_x-F_x\cos\alpha-F_y\sin\alpha)}$, $\theta(L)=\alpha$ and $\frac{\mathrm{d}\theta}{\mathrm{d}s}(L)=0$. Differentiating (19) twice ends up with the fourth-order ODE:

$$\begin{aligned}EI\frac{\mathrm{d}^4\theta}{\mathrm{d}s^4}+F_x(-\sin\theta(s)(\frac{\mathrm{d}\theta}{\mathrm{d}s})^2+\cos\theta(s)\frac{\mathrm{d}^2\theta}{\mathrm{d}s^2})\\ +F_y(\cos\theta(s)(\frac{\mathrm{d}\theta}{\mathrm{d}s})^2+\sin\theta(s)\frac{\mathrm{d}^2\theta}{\mathrm{d}s^2})=0\end{aligned} \tag{24}$$

Therefore, we can easily reach the final solution of $\theta(s)$ via solving ODE (24) constrained by the obtained boundary conditions under collocation method. If we consider the practical design that involves this post-buckling behavior, the mechanism would follow the layout as shown in Fig. 13.

3.2 Case 7: post-buckling behavior of moving revolute joints at both ends

This case actually is the post-buckling study of Case 4 as displayed in Fig. 14. Likewise, we would like to analyze the post-buckling behavior from point A through B finally to point C. The governing equation is first derived and needs to be arranged in a clear way: $EI\frac{\mathrm{d}\theta}{\mathrm{d}s} = M(s) = -F_x y(s) + \frac{F_y}{2}x(s)$. Differentiating this equation, we will obtain:

$$EI\frac{\mathrm{d}^2\theta}{\mathrm{d}s^2} = -F_x\sin\theta(s) + \frac{F_y}{2}\cos\theta(s) \tag{25}$$

Slightly manipulating (25), we then can reach:

$$\frac{1}{2}EI(\frac{\mathrm{d}\theta}{\mathrm{d}s})^2 - F_x\cos\theta(s) - \frac{F_y}{2}\sin\theta(s) = C \tag{26}$$

Substituting the boundary conditions $\theta(0) = \alpha$ and $\frac{\mathrm{d}\theta}{\mathrm{d}s}(0) = 0$ into (26) gives us:

$$C = -(F_x\cos\alpha + \frac{F_y}{2}\sin\alpha) \tag{27}$$

Similarly, substituting the boundary conditions $\theta(\frac{L}{2}) = 0$ and $\frac{\mathrm{d}\theta}{\mathrm{d}s}(\frac{L}{2})$ into (26) gives us:

$$C = \frac{1}{2}EI(\frac{\mathrm{d}\theta}{\mathrm{d}s}(\frac{L}{2}))^2 - F_x \tag{28}$$

Then, rearranging (26) and (27) yields:

$$\frac{\mathrm{d}\theta}{\mathrm{d}s} = \pm\sqrt{\frac{2F_x}{EI}(\cos\theta(s) - \cos\alpha) + \frac{F_y}{EI}(\sin\theta(s) - \sin\alpha)} \tag{29}$$

Clearly, we will have one unique solution ($\theta(s) = 0$ and $F_y = 0$) to (29) and (25). Besides, if $\alpha > 0$, we will have:

$$f(\alpha, F_y) = \int_{\alpha}^{0} \frac{-1}{\sqrt{\frac{2F_x}{EI}(\cos\theta(s) - \cos\alpha) + \frac{F_y}{EI}(\sin\theta(s) - \sin\alpha)}}\mathrm{d}\theta - \int_{0^+}^{\frac{L}{2}} \mathrm{d}s \tag{30}$$

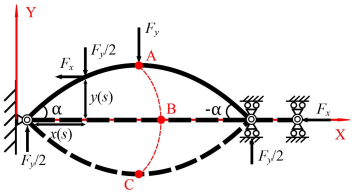

Fig. 14: Case 7: post-buckling behavior of Case 4

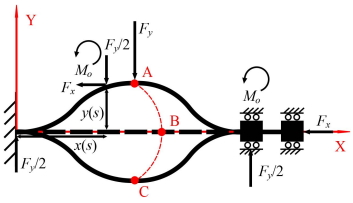

Fig. 15: Case 8: post-buckling behavior of Case 5

If α or F_y is known, it can be solved using Newton-Raphson method. Similarly, if $\alpha < 0$, we will arrive at: $f(\alpha, F_y) = \int_{\alpha^+}^{0} \frac{1}{\sqrt{\frac{2F_x}{EI}(\cos\theta(s) - \cos\alpha) + \frac{F_y}{EI}(\sin\theta(s) - \sin\alpha)}}\mathrm{d}\theta - \int_{0^+}^{\frac{L}{2}} \mathrm{d}s$. Similarly, if α or F_y is known, it can be solved using Newton-Raphson method as well. Then, we will be able to obtain the value of $\frac{\mathrm{d}\theta}{\mathrm{d}s}(\frac{L}{2})$ via dealing with (27) and (28) together:

$$\frac{\mathrm{d}\theta}{\mathrm{d}s}(\frac{L}{2}) = \mp\sqrt{\frac{1}{EI}(2F_x - 2F_x\cos\alpha - F_y\sin\alpha)} \tag{31}$$

Logically, the boundary conditions are all available: $\theta(0) = \alpha$, $\frac{\mathrm{d}\theta}{\mathrm{d}s}(0) = 0$, $\theta(\frac{L}{2}) = 0$ and $\frac{\mathrm{d}\theta}{\mathrm{d}s}(\frac{L}{2}) = \mp\sqrt{\frac{1}{EI}(2F_x - 2F_x\cos\alpha - F_y\sin\alpha)}$. Then, differentiating (25) twice gives us the final governing fourth-order ODE:

$$\begin{aligned} EI\frac{\mathrm{d}^4\theta}{\mathrm{d}s^4} + F_x(-\sin\theta(s)(\frac{\mathrm{d}\theta}{\mathrm{d}s})^2 + \cos\theta(s)\frac{\mathrm{d}^2\theta}{\mathrm{d}s^2}) \\ + \frac{F_y}{2}(\cos\theta(s)(\frac{\mathrm{d}\theta}{\mathrm{d}s})^2 + \sin\theta(s)\frac{\mathrm{d}^2\theta}{\mathrm{d}s^2}) = 0 \end{aligned} \tag{32}$$

Finally, we are able to get the solution of $\theta(s)$ via solving ODE (32) constrained by the obtained boundary conditions under collocation method. The practical design of the mechanism follows the basic structure displayed in Fig. 14.

3.3 Case 8: post-buckling behavior of moving fixed joints at both ends

This case aims to characterize the post-buckling behavior of Case 5, which is shown in Fig. 15. Here, we also consider its post-buckling process from point A through point B to point C as well. The governing equation is presented below: $EI\frac{\mathrm{d}\theta}{\mathrm{d}s} = M(s) = -F_x y(s) + \frac{F_y}{2}x(s) + M_o$. Then, we can logically reach its corresponding second-order ODE: $EI\frac{\mathrm{d}^2\theta}{\mathrm{d}s^2} = -F_x\sin\theta + \frac{F_y}{2}\cos\theta$, with the following boundary conditions: $\theta(0) = 0$, $\theta(L/2) = 0$. To solve this ODE constrained by the obtained boundary conditions, setting up appropriate initial guesses.

4 Results and discussions

In this section, the numerical results from our proposed methods are compared with FEA results for verification of both high accuracy and efficiency. First of all, the material and geometry of the studied slender beam are defined

(see Fig. 16): $E = 200 \times 10^9$ Pa and Poisson's ratio $\nu = 0.3$ (structural steel); the beam length is fixed to $L = 0.1$ m; the initial parameters of the rectangular cross section are set as $w(0) = 0.006$ m and $h(0) = 0.001$ m respectively. Besides,

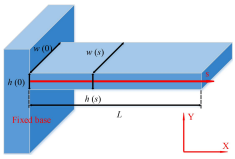

Fig. 16: The geometry of studied beam

the cross section parameters at any random point along s axis (beam axis) are noted as functions of s: $w(s)$ and $h(s)$, so the second moment inertia of the cross section area at s can be expressed as $I(s) = \frac{h(s)^3 w(s)}{12}$. Note that in Case 3 (the varying cross section case), $w(s) = (1-5s)w(0)$ and $h(s) = (1-5s)h(0)$, so $I(s) = \frac{h(s)^3 w(s)}{12} = \frac{h(0)^3 w(0)}{12}(1-5s)^4$. In the rest cases, $I(s) = \frac{h(s)^3 w(s)}{12} = \frac{h(0)^3 w(0)}{12}$.

4.1 Buckling behavior

4.1.1 Case 1: classic buckling problem

The corresponding results of F_x against $x(L)$, F_x against $y(L)$ and F_x against α are displayed in Fig. 18 (the bifurcation diagrams). The mesh information is presented below: 150 cuboid mesh elements; 216 edge elements; 408 mesh vertices. In terms of computational expense, t_{CM} and t_{FEA} refer to the time cost by collocation method and FEA respectively: $t_{CM} = 60$ s; $t_{FEA} = 5289$ s; $\frac{t_{FEA}}{t_{CM}} = \frac{5289}{60} = 88.15$.

4.1.2 Case 2: classic buckling problem with gravity

The gravity in this case can be considered as a uniformly distributed load along the beam, so $q_x(s) = \frac{G}{L} = \frac{mg}{L} = \frac{Lw(s)h(s)\rho g}{L} = w(0)h(0)\rho g = 0.46$ N/m, where G denotes the gravity exerted on the beam; m denotes the mass of the beam; g denotes the acceleration of gravity; $\rho = 7850\,\mathrm{kg/m^3}$ is density of the beam. The bifurcation diagrams of F_x against $x(L)$, F_x against $y(L)$ and F_x against α are displayed in Fig. 19. The mesh information is presented below: 150 cuboid mesh elements; 216 edge elements; 408 mesh vertices. The following presents the time cost of collocation method and FEA respectively: $t_{CM} = 24$ s; $t_{FEA} = 7524$ s; $\frac{t_{FEA}}{t_{CM}} = \frac{7524}{24} = 313.50$.

4.1.3 Case 3: classic buckling problem considering uniformly varying cross section

In this case, a slender beam of uniformly varying cross section is studied (see Fig. 17). As mentioned before, the second moment of inertia of the cross section area is formulated as: $I(s) = \frac{h(s)^3 w(s)}{12} = \frac{h(0)^3 w(0)}{12}(1-5s)^4$. The bifurcation diagrams of F_x against $x(L)$, F_x against $y(L)$ and F_x against α are displayed in Fig. 20. The mesh information is presented below: 150 Hexahedron mesh elements; 236 edge elements; 416 mesh vertices. The following presents the time cost of collocation method and FEA respectively: $t_{CM} = 20$ s; $t_{FEA} = 4020$ s; $\frac{t_{FEA}}{t_{CM}} = \frac{4020}{20} = 201$.

4.1.4 Case 4: classic buckling problem about moving revolute joints at the both ends

Here, the results of the first-order and second-order buckling behaviors are presented. The mesh information is presented below: 150 cuboid mesh elements; 216 edge elements; 408 mesh vertices.

* First-order buckling: the bifurcation diagrams of F_x against $x(L/2)$, F_x against $y(L/2)$ and F_x against α are displayed in Fig. 21. The following presents the time cost of collocation method and FEA respectively: $t_{CM} = 13$ s; $t_{FEA} = 4320$ s; $\frac{t_{FEA}}{t_{CM}} = \frac{4320}{20} = 332.31$.
* Second-order buckling: the bifurcation diagrams of F_x against $x(L/4)$, F_x against $y(L/4)$ and F_x against α are displayed in Fig. 22. The following presents the time cost of collocation method and FEA respectively: $t_{CM} = 40$ s; $t_{FEA} = 69$s; $\frac{t_{FEA}}{t_{CM}} = \frac{69}{40} = 1.73$.

4.1.5 Case 5: classic buckling problem about moving fixed constraints at the both ends

The bifurcation diagrams of F_x against $x(L/2)$, F_x against $y(L/2)$ and F_x against α are displayed in Fig. 23. The mesh information is presented below: 150 cuboid mesh elements; 216 edge elements; 408 mesh vertices. The following presents the time cost of collocation method and FEA respectively: $t_{CM} = 7$ s; $t_{FEA} = 62$ s; $\frac{t_{FEA}}{t_{CM}} = \frac{62}{7} = 8.85$.

4.1.6 Discussions

Obviously, the results displayed in Figs. 18 to 23 prove that our numerical method can effectively catch the characteristics of buckling behaviors in different cases. Besides, the computational cost is shown to be much less than FEA. Therefore, both in terms of accuracy and efficiency, our proposed method have demonstrated dominant advantages in characterizing the buckling behavior of slender beams. As we can notice, buckling behaviors of slender flexible structures provide unpredictably promising possibilities for designing CMs due to their nonlinear/large deformation and complex mechanical responses. Several CM designs noted in the literature (such as multi-stable mechanisms) have intuitively included the buckling phenomenon to some extent. However, to the best of our knowledge, nearly no contributions to theoretically modeling buckling behaviors directly based on geometrically nonlinear Euler–Bernoulli beam theory have ever been made in the field of CMs. In other words, our proposed method can serve as a universal and effective

Fig. 17: The geometry of studied beam in Case 3

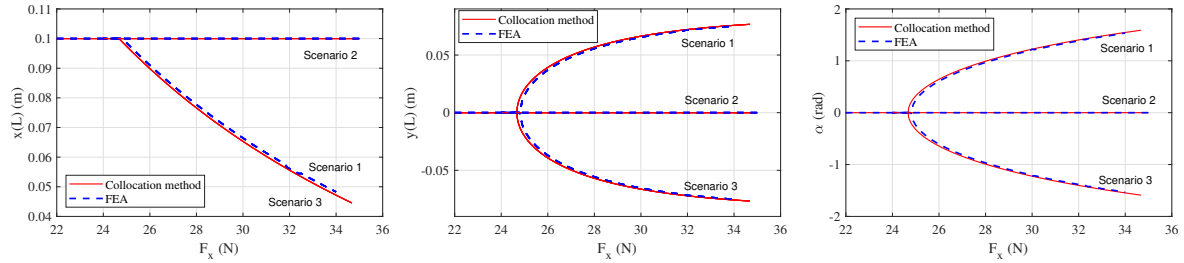

(a) F_x - $x(L)$ (b) F_x - $y(L)$ (c) F_x - α

Fig. 18: Bifurcation diagrams of Case 1

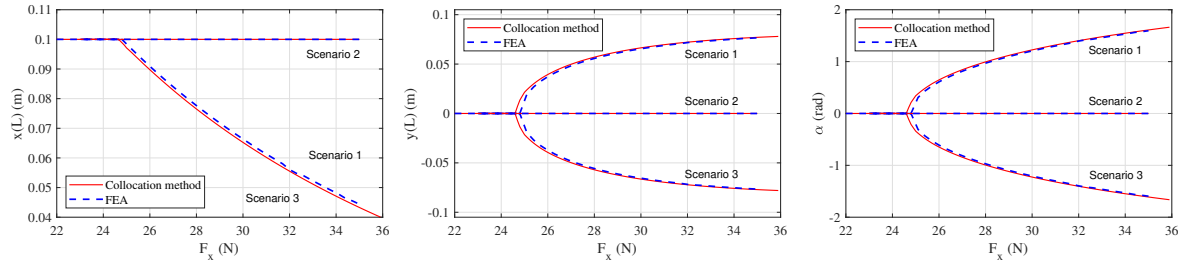

(a) F_x - $x(L)$ (b) F_x - $y(L)$ (c) F_x - α

Fig. 19: Bifurcation diagrams of Case 2

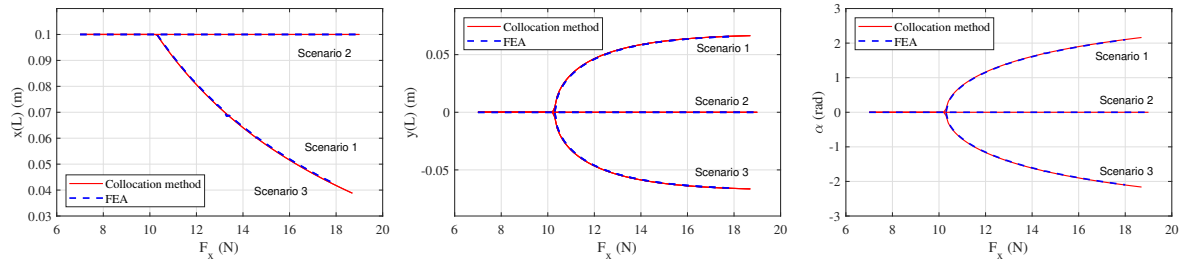

(a) F_x - $x(L)$ (b) F_x - $y(L)$ (c) F_x - α

Fig. 20: Bifurcation diagrams of Case 3

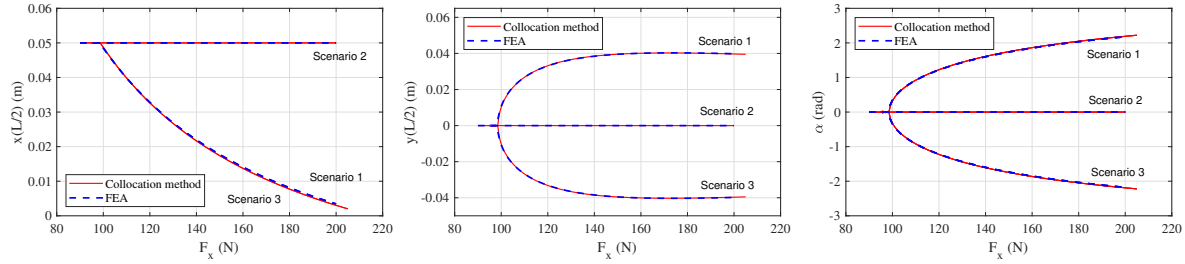

(a) F_x - $x(L/2)$ (b) F_x - $y(L/2)$ (c) F_x - α

Fig. 21: Bifurcation diagrams of Case 4 (first-order buckling)

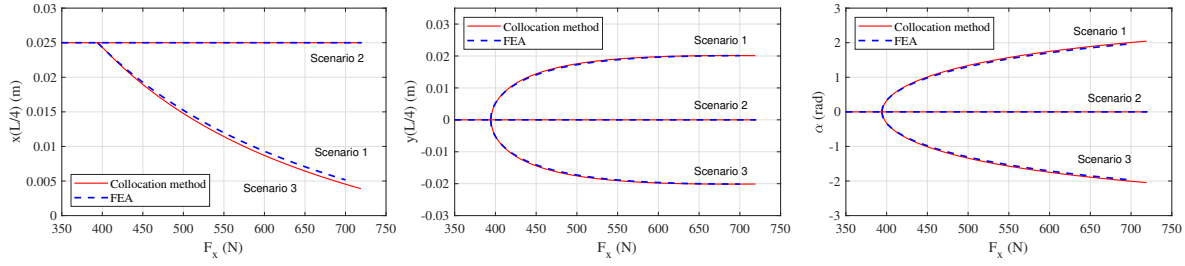

(a) F_x - $x(L/4)$ (b) F_x - $y(L/4)$ (c) F_x - α

Fig. 22: Bifurcation diagrams of Case 4 (second-order buckling)

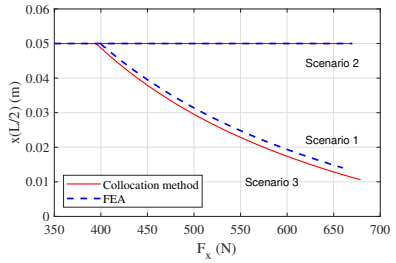

(a) F_x - $x(L/2)$

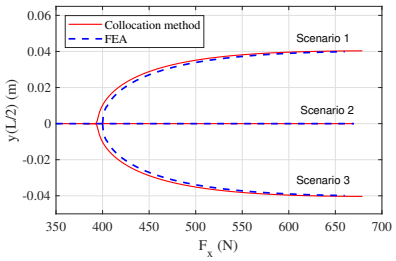

(b) F_x - $y(L/2)$

Fig. 23: Bifurcation diagrams of Case 5

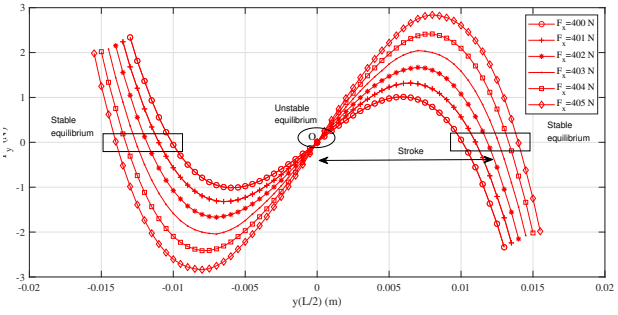

Fig. 24: Insight study on Case 8: $y(L/2)$ - F_y relationship

tool to solve the mentioned problems as well as assisting buckling-involved CM designs.

4.2 Post-buckling behavior

In Chapter. 1.3, we have proved that the operational process of bi-stable mechanisms are essentially post-buckling behaviors. Therefore, it is worth discovering if the post-buckling behaviors of the studied cases (Case 6 to Case 8) have anything in common with the traditional bi-stable mechanisms. To do that, the force-displacement plots are a graphically straightforward tool [14], which can intuitively present the mechanical responses of studied bi-stable mechanisms. The results are also displayed in a similar manner as follows. Here in this section, an insight study on Case 8 is presented.

4.2.1 Case 6: post-buckling behavior of a fixed constraint at one end

Fig. 25 demonstrates the relationship between $y(L)$ and F_y under three different axial forces $F_x = 30, 32, 34\,\mathrm{N}$ where

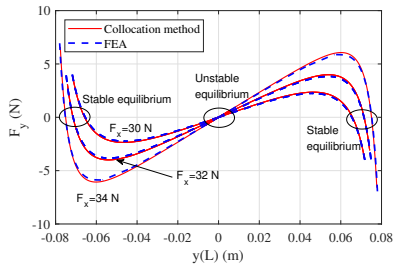

Fig. 25: $y(L)$ - F_y relationship in Case 6

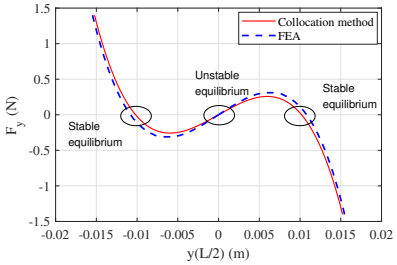

Fig. 26: $y(L/2)$ - F_y relationship in Case 7

the results obtained from FEA and the proposed collocation method are compared. The mesh information is presented below: 150 cuboid mesh elements; 216 edge elements; 408 mesh vertices. The computational expenses of the mentioned methods are presented respectively: $t_{CM} = 40$ s; $t_{FEA} = 1794$ s; $\frac{t_{FEA}}{t_{CM}} = \frac{1794}{40} = 45.85$.

4.2.2 Case 7: post-buckling behavior of moving revolute joints at both ends

In this section, the force-displacement plot of first-order post-buckling behavior of the studied slender beam is presented. Fig. 26 demonstrates the relationship between $y(L/2)$ and F_y under a fixed axial force $F_x = 100\,\mathrm{N}$ where the results obtained from FEA and the proposed collocation method are compared. The mesh information is presented below: 150 cuboid mesh elements; 216 edge elements; 408 mesh vertices. The computational expenses of the mentioned methods are presented respectively: $t_{CM} = 7$ s; $t_{FEA} = 206$ s; $\frac{t_{FEA}}{t_{CM}} = \frac{206}{7} = 29.42$.

4.2.3 Discussions

According to the results shown above (Fig. 25 and Fig. 26), our proposed method can effectively catch the characteristics of post-buckling behavior in different cases, and the computational expense is much less than FEA as well. As shown in Fig. 25, the mechanical responses of the studied mechanism are dependent of the axial force F_x. Besides, Fig. 25 and Fig. 26 have also clearly demonstrated the stable and unstable equilibrium (buckling initiation) states of the studied mechanisms. These mentioned interesting characteristics have triggered our next-step theoretical exploration where Case 8 is studied as an example.

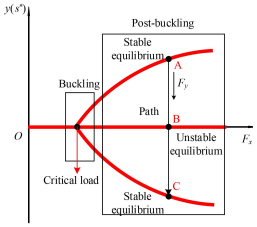

Fig. 27: State transformation of the studied mechanism in Case 8 (also valid for Cases 6 and 7)

4.3 Theoretical insights

This section aims to theoretically analyze the mechanical properties of the mechanisms (Cases 6-8) proposed in this paper where Case 8 is taken as a representative case here, providing design insights for future work. Let's take a look at the following characteristics (obtained by collocation method) of the studied mechanism as demonstrated in Fig. 24:

1 The force-displacement plot (Fig. 24) is totally symmetric with respect to the unstable equilibrium point O, which is similar to odd functions. Obviously, O also refers to the buckling initiation state of the mechanism.
2 The stiffness K of this post-buckling process is defined as $K = -\dfrac{\Delta F_y}{\Delta y(L/2)}$ so it's obvious that the mechanism has two stable equilibrium points shown in Fig. 24.
3 Here, we define the distance between the unstable equilibrium point and one stable equilibrium point as the *Stroke* (S) of the mechanism.
4 The mechanical properties of the mechanism depends on the axial force F_x, which can be controlled by users. As F_x gets smaller, the stable equilibrium points gradually come to approach the unstable equilibrium point O. When F_x decreases below the critical load (first-order buckling load), the system will just have one equilibrium point, which is stable and located at O. In this situation, the slender beam does not experience buckling initiation at all, demonstrated in Fig. 27
5 As shown in Fig. 27, the mechanism follows the path A-B-C driven by the vertical load F_y to fulfill state jumping, which is perfectly symmetric compared to Fig. 6.

Concluded from the mentioned above, we would like to term the mechanism proposed in Case 8 (also valid in Case 6 and Case 7) as **Pre-buckled Bi-stable Mechanisms (PBMs)**. Compared with the classic bi-stable mechanisms, the advantages of PBMs lie in:

1 To the best of our knowledge, PBMs take the lead to combine the use of rigid and compliant mechanisms, which provides the chance for users to make most of merits of the mentioned two types of mechanisms.
2 PBMs gracefully remain the intrinsic beauty of CMs: *symmetry* [4], which enables themselves to be more reconfigurable and maneuverable in certain applications.
3 PBMs are easily adjustable to re-set its mechanical responses simply by tuning the axial force F_x whereas the classic ones need to be pre-fabricated and are always fixed to one single setting.
4 Also, the stiffness K and the stroke S can be straightforwardly optimized via setting up objective functions where F_x could be the optimized variables (or the geometric parameters of the PBM).
5 PBMs are open to be reconstructed through simple ways. For example, the operational path A-B-C of Case 7 is curved (see Fig. 14), which is not convenient for practical implementation. To solve this inconvenience, two springs with same stiffness are added in a simple manner to straighten the path, demonstrated in Fig. 28.

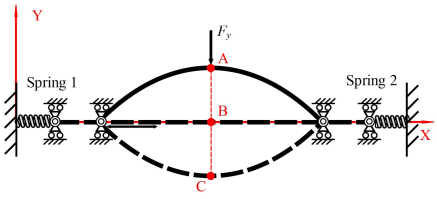

Fig. 28: Optimized concept design of Case 7

5 Conclusions

Compliant Mechanisms have been attracting talented researchers in recent years, presenting many desired mechanical properties. In this paper, we characterize eight cases of nonlinear buckling and post-buckling behaviors via numerically approximating the geometrically nonlinear solution of the famous Euler–Bernoulli beam theory. We then propose a novel type of bi-stable mechanisms termed as Pre-buckled Bi-stable Mechanisms (PBMs) that integrate the features of both rigid and compliant mechanisms, followed by detailed theoretical insights. The work of this paper provides theoretical and numerical results, which can be used to conduct mechanism optimization. Our future work will include practical designs of PBMs for some certain applications based on the theoretical contributions achieved in this paper.

Acknowledgment

This work is partially supported by the National Natural Science Foundation of China (Grant No. 62073081), by the Project of Department of Education of Guangdong Province (Grant No. 2019KZDXM037), by the fund of Guangdong-Hong Kong-Macao Joint Laboratory for Intelligent Micro-Nano Optoelectronic Technology (No. 2020B1212030010), by the project ROBOCOP [ANR-19-CE19], by the project COSSEROOTS [ANR-20-CE33], by the project Inventor (I-SITE ULNE, le programme d'Investissements d'Avenir, Métropole Européenne de Lille), France .

References

[1] Larry L Howell. Compliant mechanisms. In 21st century kinematics. Springer, London, 2013.
[2] Nicolae Lobontiu. Compliant mechanisms: design of flexure hinges. CRC press, Boca Raton, 2020.

[3] D Farhadi Machekposhti, N Tolou, and JL Herder. A review on compliant joints and rigid-body constant velocity universal joints toward the design of compliant homokinetic couplings. Journal of Mechanical Design, 137(3), 2015.

[4] Shorya Awtar. Synthesis and analysis of parallel kinematic XY flexure mechanisms. PhD thesis, Massachusetts Institute of Technology, 2003.

[5] Young Seok Oh and Sridhar Kota. Synthesis of multistable equilibrium compliant mechanisms using combinations of bistable mechanisms. Journal of Mechanical Design, 131(2), 2009.

[6] Piyu Wang and Qingsong Xu. Design and modeling of constant-force mechanisms: A survey. Mechanism and Machine Theory, 119:1–21, 2018.

[7] Sridhar Kota, Jinyong Joo, Zhe Li, Steven M Rodgers, and Jeff Sniegowski. Design of compliant mechanisms: applications to mems. Analog integrated circuits and signal processing, 29(1):7–15, 2001.

[8] Lael U Odhner and Aaron M Dollar. The smooth curvature model: An efficient representation of euler–bernoulli flexures as robot joints. IEEE Transactions on Robotics, 28(4):761–772, 2012.

[9] Jonathan Granstrom, Joel Feenstra, Henry A Sodano, and Kevin Farinholt. Energy harvesting from a backpack instrumented with piezoelectric shoulder straps. Smart Materials and Structures, 16(5):1810, 2007.

[10] Anzhu Gao, Yuanyuan Zhou, Lei Cao, Zhidong Wang, and Hao Liu. Fiber bragg grating-based triaxial force sensor with parallel flexure hinges. IEEE Transactions on Industrial Electronics, 65(10):8215–8223, 2018.

[11] Robert Millard Jones. Buckling of bars, plates, and shells. Bull Ridge Corporation, 2006.

[12] Don O Brush, Bo O Almroth, and JW Hutchinson. Buckling of bars, plates, and shells. 1975.

[13] Stephen P Timoshenko and James M Gere. Theory of elastic stability. Courier Corporation, 2009.

[14] Guimin Chen and Fulei Ma. Kinetostatic modeling of fully compliant bistable mechanisms using timoshenko beam constraint model. Journal of Mechanical Design, 137(2), 2015.

[15] Leonhard Euler. Methodus inveniendi lineas curvas maximi minimive proprietate gaudentes. apud Marcum-Michaelem Bousquet, 1744.

[16] Joseph-Louis Lagrange. Sur la figure des colonnes. Miscellanea Taurinensia, 5:123–166, 1770.

[17] Isaac Todhunter. A History of the Theory of Elasticity and of the Strength of Materials: pts. 1-2. Saint-Venant to Lord Kelvin, volume 2. University Press, 1893.

[18] S-N Chow and Jack K Hale. Methods of bifurcation theory, volume 251. Springer Science & Business Media, 2012.

[19] Stuart Antman. Nonlinear Problems of Elasticity; 2nd ed. Springer, Dordrecht, 1996.

[20] Walter Lacarbonara. Buckling and post-buckling of non-uniform non-linearly elastic rods. International Journal of Mechanical Sciences, 50(8):1316–1325, 2008.

[21] G Domokos, P Holmes, and B Royce. Constrained euler buckling. In Mechanics: From Theory to Computation, Journal of Nonlinear Science, pages 413–446. Springer, 2000.

[22] Samir Emam and Walter Lacarbonara. Buckling and postbuckling of extensible, shear-deformable beams: Some exact solutions and new insights. International Journal of Non-Linear Mechanics, 129:103667, 2021.

[23] Zhangxian Yuan and Xinwei Wang. Buckling and post-buckling analysis of extensible beam–columns by using the differential quadrature method. Computers & Mathematics with Applications, 62(12):4499–4513, 2011.

[24] BJ Hansen, CJ Carron, BD Jensen, AR Hawkins, and SM Schultz. Plastic latching accelerometer based on bistable compliant mechanisms. Smart Materials and Structures, 16(5):1967, 2007.

[25] Matthew R Brake, Michael S Baker, Nathan W Moore, Douglas A Crowson, John A Mitchell, and Jack E Houston. Modeling and measurement of a bistable beam in a microelectromechanical system. Journal of microelectromechanical systems, 19(6):1503–1514, 2010.

[26] Troy Gomm, Larry L Howell, and Richard H Selfridge. In-plane linear displacement bistable microrelay. Journal of Micromechanics and Microengineering, 12(3):257, 2002.

[27] Moustapha Hafez, Matthew D Lichter, and Steven Dubowsky. Optimized binary modular reconfigurable robotic devices. IEEE/ASME transactions on mechatronics, 8(1):18–25, 2003.

[28] Martín A Pucheta and Alberto Cardona. Design of bistable compliant mechanisms using precision–position and rigid-body replacement methods. Mechanism and Machine Theory, 45(2):304–326, 2010.

[29] Bruno Ando, Salvatore Baglio, Gaetano L'Episcopo, and Carlo Trigona. Investigation on mechanically bistable mems devices for energy harvesting from vibrations. Journal of Microelectromechanical Systems, 21(4):779–790, 2012.

[30] RD Russell and Lawerence F Shampine. A collocation method for boundary value problems. Numerische Mathematik, 19(1):1–28, 1972.

[31] Lawrence F Shampine, Jacek Kierzenka, Mark W Reichelt, et al. Solving boundary value problems for ordinary differential equations in matlab with bvp4c. Tutorial notes, 2000:1–27, 2000.

[32] Joseph Frederick Traub. Iterative methods for the solution of equations, volume 312. American Mathematical Soc., 1982.

[33] Anne Greenbaum. Iterative methods for solving linear systems. SIAM, 1997.